Supporting information for:

Understanding the evolution of ternary alloyed nanoparticles during reversible exsolution from double perovskite oxides

Andrés López-García[1], Alfonso J. Carrillo[1*], Catalina E. Jiménez[2], Rosario Suarez Anzorena[2,3], Raul Garcia-Diez[2], Virginia Pérez-Dieste[4], Ignacio J. Villar-Garcia[4,5], Ana B. Hungría[6], Marcus Bär[2,7,8], José M. Serra[1*]

[1]*Instituto de Tecnología Química, (Universitat Politècnica de València-Consejo Superior de Investigaciones Científicas), Valencia, Spain*

[2]*Dept. Interface Design, Helmholtz-Zentrum Berlin für Materialien und Energie GmbH (HZB), Albert-Einstein-Str.15, 12489, Berlin, Germany*

[3]*Unidad de Investigación y Desarrollo Estratégico para la Defensa (UNIDEF-CONICET-MINDEF), CITEDEF, J.B. de La Salle 4397, Buenos Aires, Argentina*

[4]*ALBA Synchrotron, Carrer de la Llum 2-26, 08290 Barcelona, Spain.*

[5]*Universidad CEU San Pablo, Facultad de Farmacia, Departamento de Química, Urbanización Montepríncipe, 28668 Boadilla del Monte, Madrid, Spain.*

[6]*Departamento de Ciencia de Materiales, Ingeniería Metalúrgica y Química Inorgánica, Universidad de Cádiz, Campus Río San Pedro, 11510 Puerto Real, Spain.*

[7]*Dept. X-ray Spectroscopy at Interfaces of Thin Films, Helmholtz-Institute Erlangen-Nürnberg for Renewable Energy (HI ERN), Albert-Einstein-Str. 15, 12489 Berlin, Germany*

[8]*Department of Chemistry and Pharmacy, Friedrich-Alexander-Universität Erlangen-Nürnberg (FAU), Egerlandstr. 3, 91058 Erlangen, Germany*

Corresponding authors: jmserra@itq.upv.es; alcardel@itq.upv.es

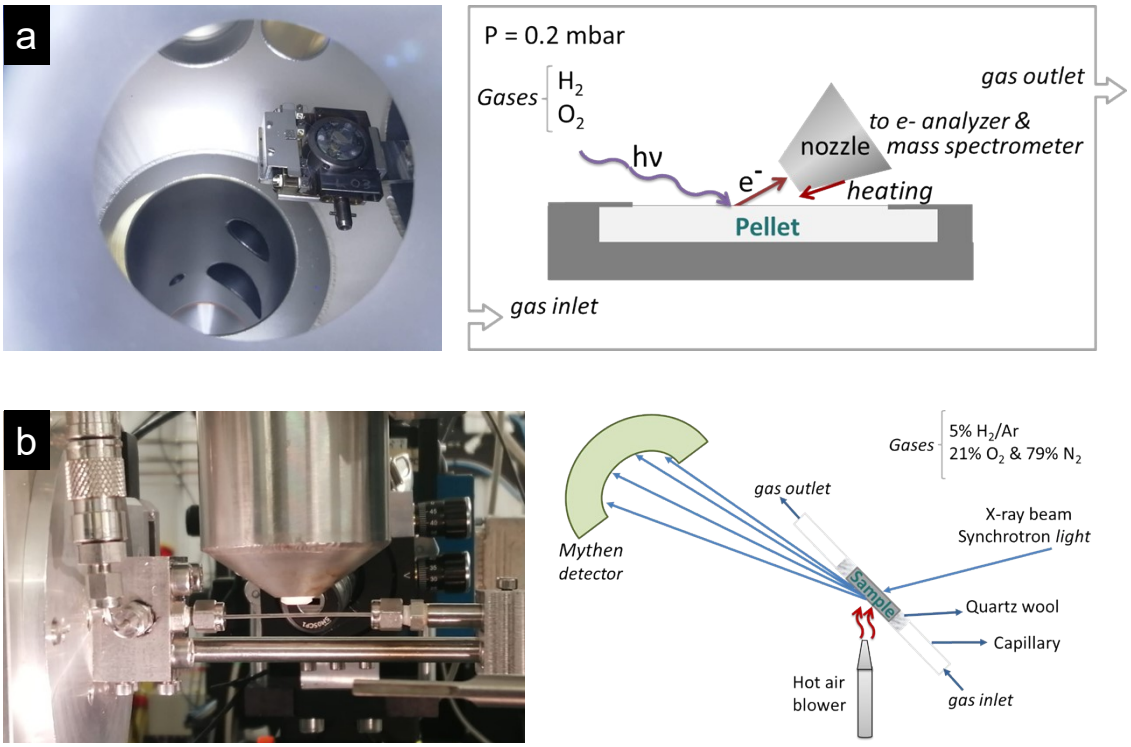

Figure S1. (a) NAP-XPS chamber picture and detailed schematic with the sample holder and the perovskite oxide pellet. **(b)** Setup picture and detailed schematic for measuring in-situ XRD showing the quartz capillaries and the hot air gun.

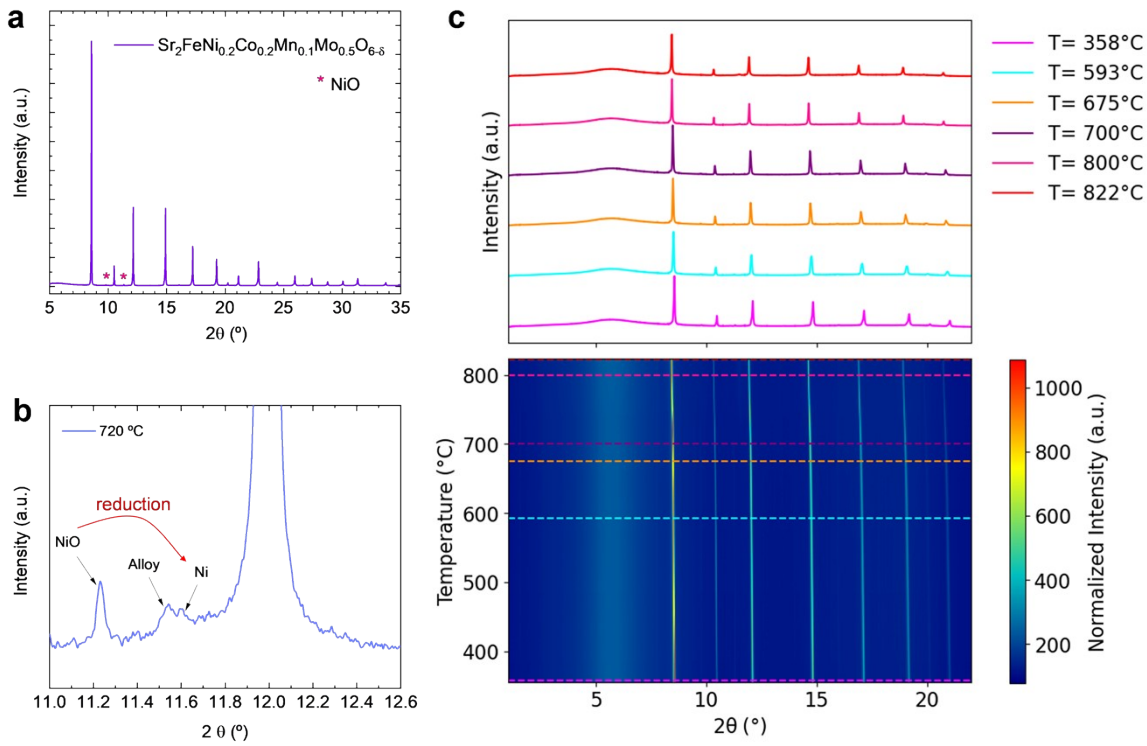

Figure S2. (a) X-ray diffractogram of pristine $Sr_2FeCo_{0.2}Ni_{0.2}Mn_{0.1}Mo_{0.5}O_{6-\delta}$, showing the minor presence of NiO. **(b)** XRD diffractogram collected at 720 ºC under 5% H_2/Ar flow, exhibiting a double metallic signal ("Alloy" & "Ni"). Diffractograms taken at different temperatures showing the whole 2θ range and a contour plot depicting the evolution of the observed reflections **(c)**.

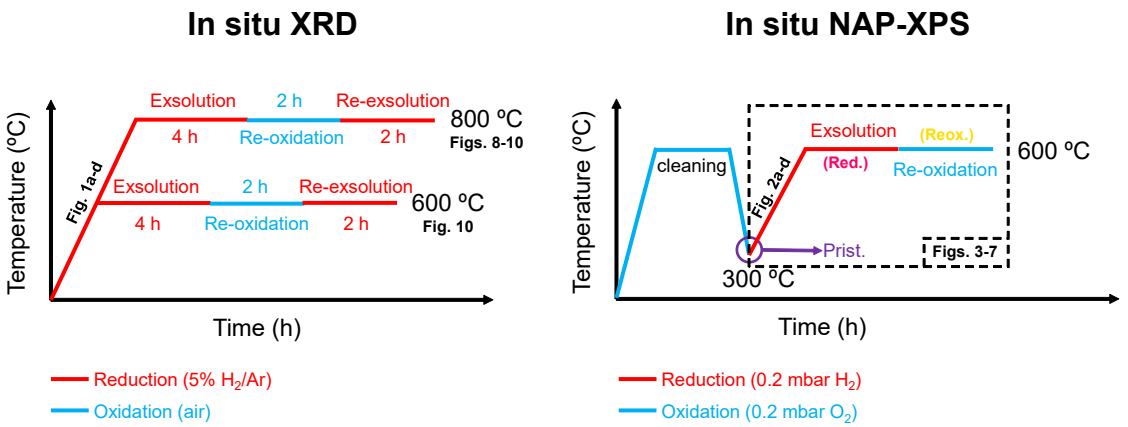

Figure S3. Temperature-time measuring protocols for the XRD (left) and NAP-XPS (right) measurements employed for in-situ analyzing the formation of exsolved ternary alloyed NPs.

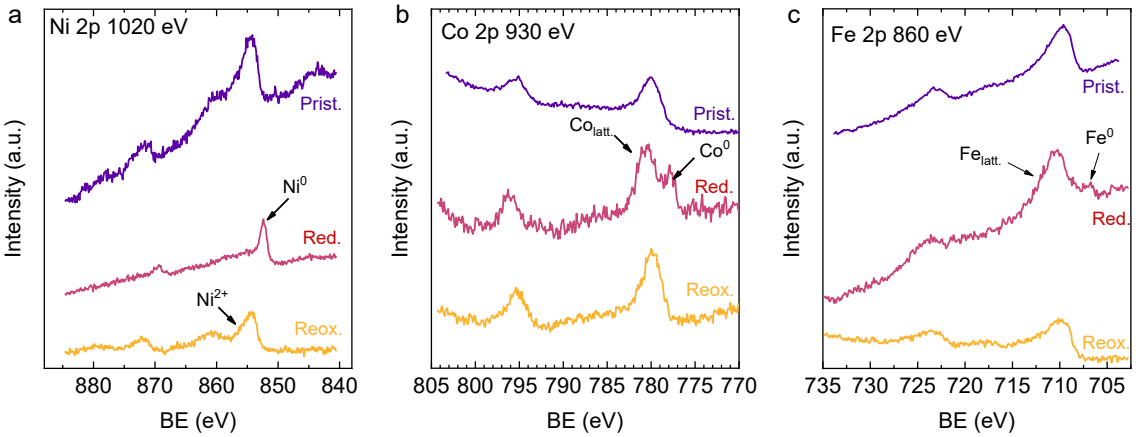

Figure S4. NAP-XPS spectra of **(a)** Ni 2p **(b)** Co 2p, and **(c)** Fe 2p core levels acquired *in-situ* at 600 ºC in pristine ("Prist.", 0.2 mbar O_2), reduced ("Red.", 0.2 mbar H_2) and re-oxidized ("Reox.", 0.2 mbar O_2) conditions. The used photon energies (to result in a similar electron kinetic energy of 150 eV) are indicated in the panels. A constant offset for better clarity is added to the spectra.

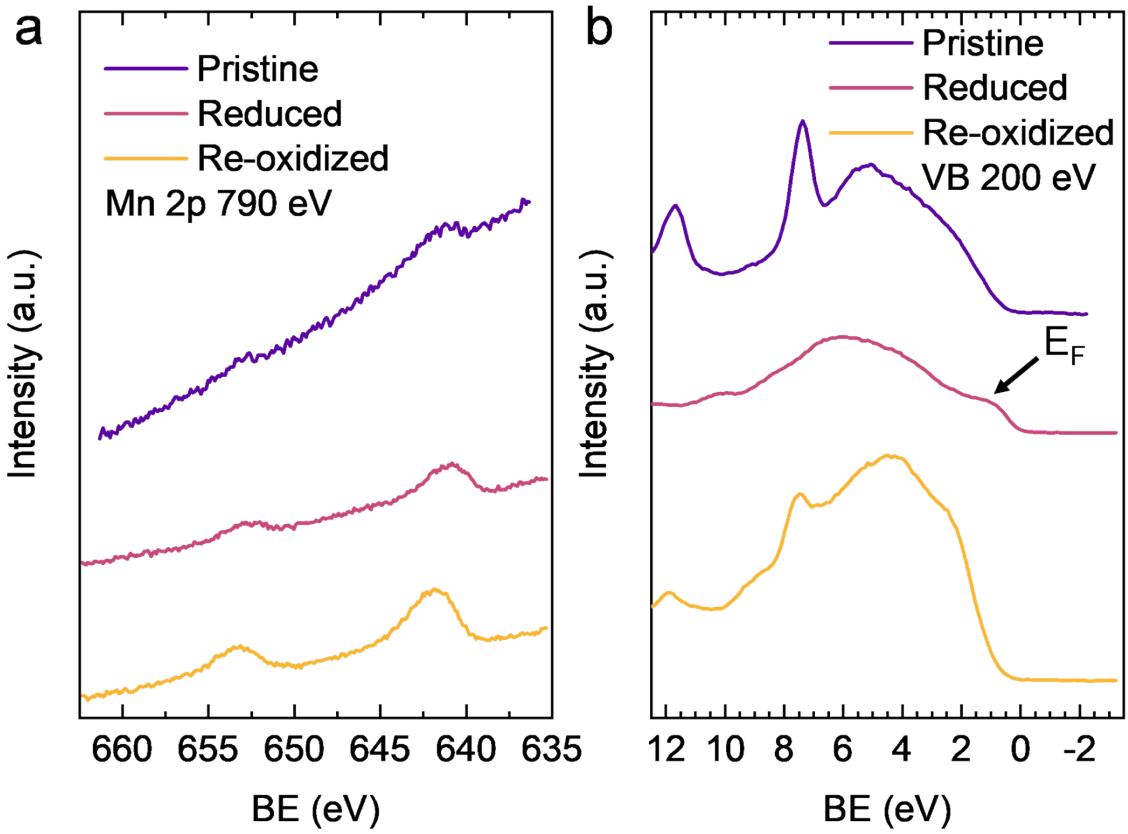

Figure S5. NAP-XPS spectra of **(a)** Mn 2p core level and **(b)** the valence band (VB) region acquired in-situ at 600 ºC in pristine (0.2 mbar O_2), reduced (0.2 mbar H_2) and re-oxidized (0.2 mbar O_2) conditions. E_F indicates the position of the Fermi level (E_F) in panel (b). Used photon energies are indicated in the panels. Constant offset added for clarity.

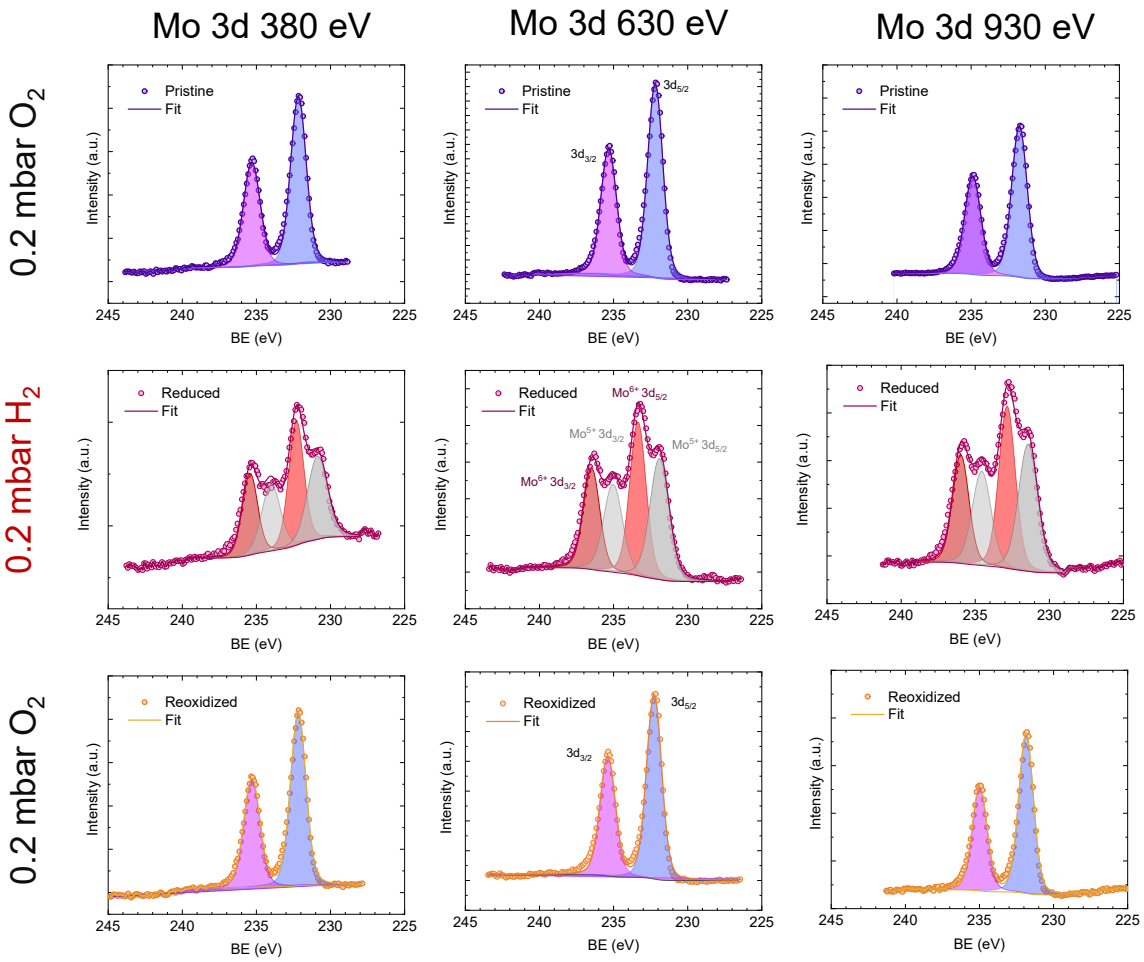

Figure S6. NAP-XPS fitted spectra of Mo 3d at the pristine (0.2 mbar O_2), reduced (0.2 mbar H_2), and re-oxidized (0.2 mbar O_2) sample states using three photon energies: 380, 630 and 930 eV. The spectra of the reduced sample show the presence of both, Mo^{5+} and Mo^{6+}, whereas in the pristine and oxidized sample states only Mo^{6+} is present.

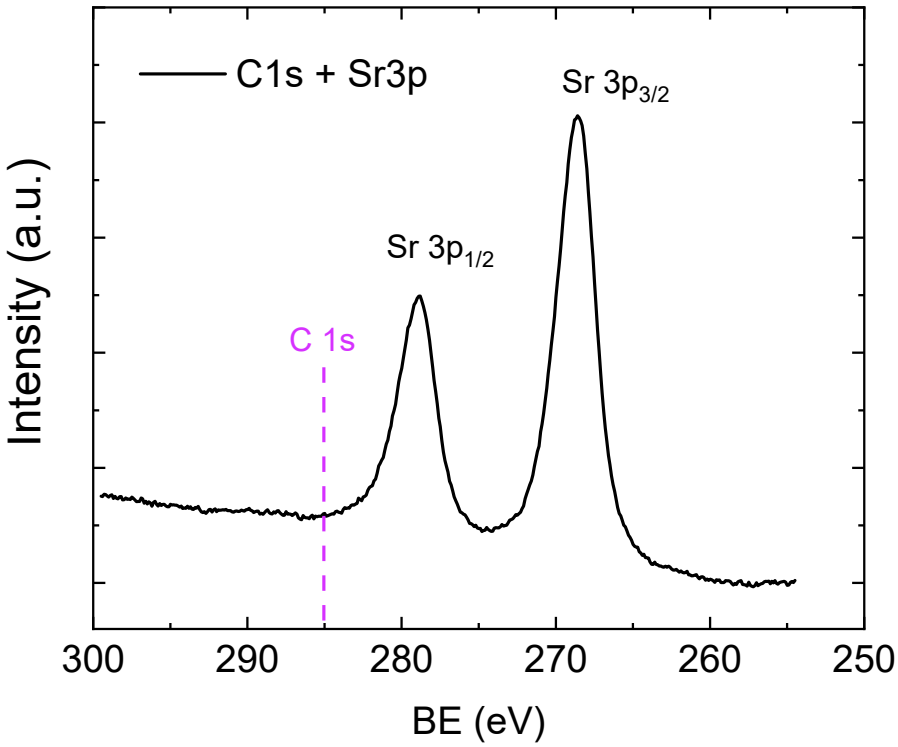

Figure S7. NAP-XPS spectra of the (overlapping) C 1s and Sr 3p core level regions of $Sr_2FeCo_{0.2}Ni_{0.2}Mn_{0.1}Mo_{0.5}O_{6-\delta}$ sample in the pristine sample state. Data acquired with a photon energy of 1030 eV. The visible spin-orbit doublet corresponds to the Sr 3p core level, whereas the C 1s line around 284.8 eV is not observed, indicating successful carbon-based species removal during the initial heating cleaning process.

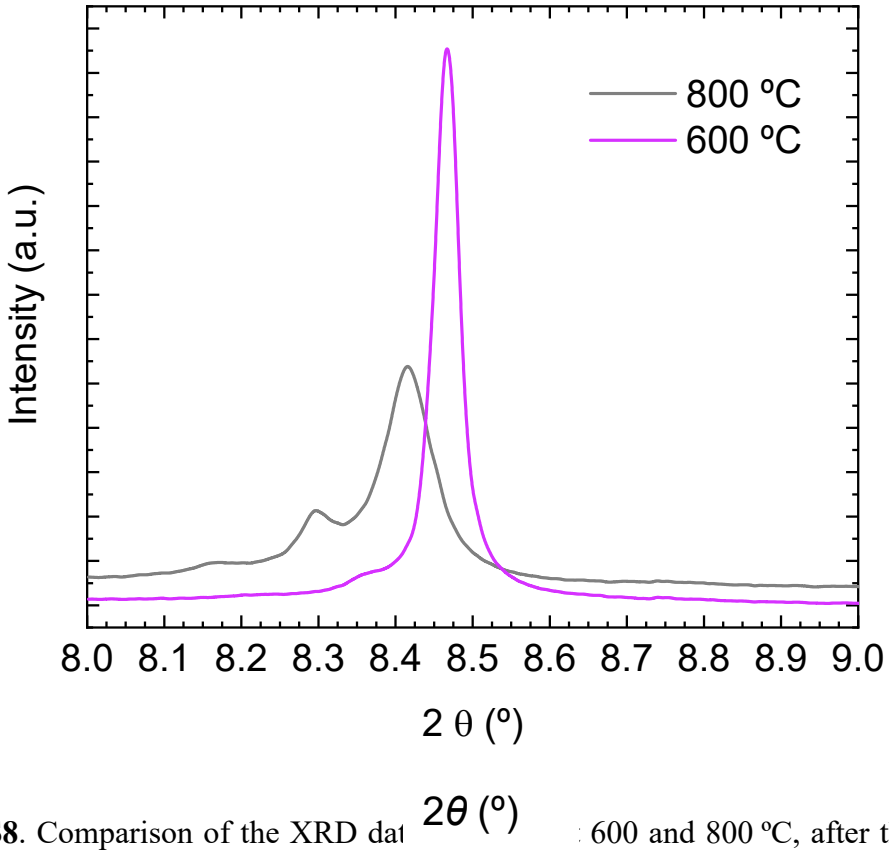

Figure S8. Comparison of the XRD dat 600 and 800 ºC, after the second reduction treatment, consisting of 2 h under 5 % H_2/Ar for $Sr_2FeCo_{0.2}Ni_{0.2}Mn_{0.1}Mo_{0.5}O_{6-\delta}$ main reflection (2 0 0) region.

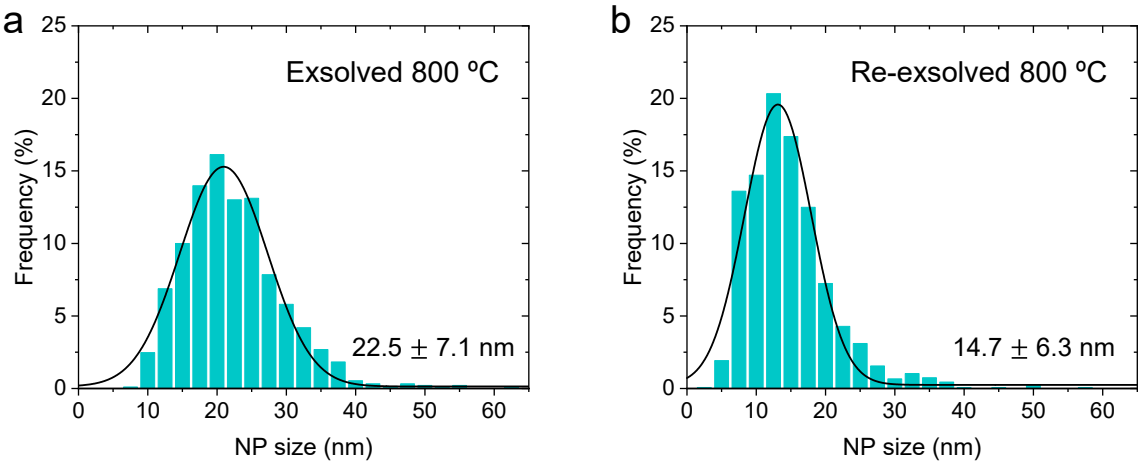

Figure S9. Histograms for the size distribution of the exsolved NPs for $Sr_2FeCo_{0.2}Ni_{0.2}Mn_{0.1}Mo_{0.5}O_{6-\delta}$, after ex-situ first exsolution **(a)** and re-exsolution of the re-oxidized material **(b)**. Both reduction treatments were performed at 800 ºC, 4 h and under 5% H_2/Ar flow.

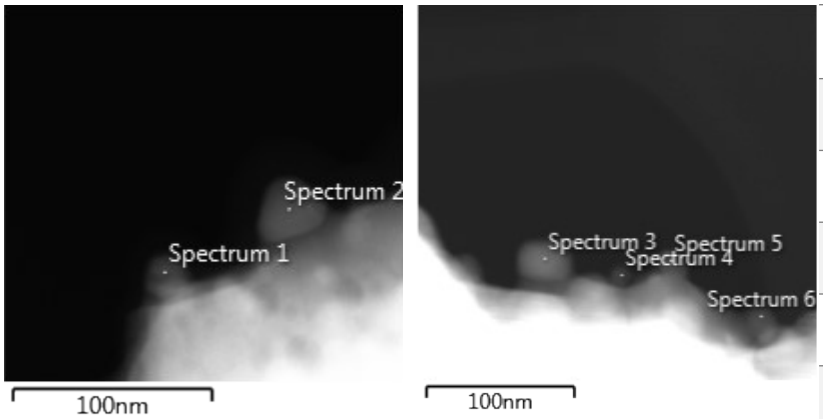

NP	Co %	Fe %	Ni %
1	31.35	46.07	22.58
2	19.49	47.35	33.16
3	30.94	43.42	25.64
4	27.15	47.85	25.00
5	23.18	49.64	27.18
6	31.15	49.10	19.75
Mean	**27.2 ± 4.9**	**47.3 ± 2.3**	**25.5 ± 4.5**

Figure S10. HAADF images of $Sr_2FeCo_{0.2}Ni_{0.2}Mn_{0.1}Mo_{0.5}O_{6-\delta}$ after ex-situ re-exsolution of the re-oxidized material. Reduction treatment was performed at 800 ºC, 4 h and under 5% H_2/Ar flow, after 24 h re-oxidation under air flow and 800 ºC. The table shows the compositional fractions of the re-exsolved NPs, where Fe becomes the main component of the ternary alloy instead of Ni.